

Rashba coupling and magnetic order in correlated helical liquids

Martin Hohenadler and Fakher F. Assaad

Institut für Theoretische Physik und Astrophysik, Universität Würzburg, Am Hubland, 97074 Würzburg, Germany

(Dated: December 30, 2014)

We study strongly correlated helical liquids with and without Rashba coupling using quantum Monte Carlo simulations of the Kane-Mele model with a Hubbard interaction at the edge. Independent of the Rashba coupling, we find that interactions enhance spin correlations and suppress the spectral weight at the Fermi level. For sufficiently strong interactions, a gap can be observed in the single-particle spectral function. However, based on a finite-size scaling analysis and theoretical arguments, we argue that this gap is closed by order parameter fluctuations in the Luttinger liquid phase even at zero temperature, and filled in by thermally induced kinks in the order parameter in the Mott phase at finite temperatures. While the bosonization suggests an umklapp-driven Mott transition only in the presence of Rashba coupling and hence a significant impact of the latter, our numerical results are almost unaffected by Rashba coupling even at low temperatures.

PACS numbers: 03.65.Vf, 71.10.Pm, 71.27+.a, 71.30.+h

I. INTRODUCTION

Helical edge states are a hallmark feature of quantum spin Hall insulators [1, 2]. In the absence of electronic correlations, there is a direct (bulk-boundary) correspondence between the number of helical edge state pairs and the Z_2 topological invariant [1]. Each pair forms a Kramers doublet related by time-reversal symmetry, with a symmetry-protected crossing at one of the two time-reversal invariant points in the Brillouin zone. A single pair of edge states is therefore stable with respect to disorder and weak interactions. The (nearly) quantized spin Hall conductivity can be used to detect the topological state in experiments [3–5].

The interplay of a topological band structure and electronic correlations has emerged as a very fruitful and active field of research. For a sufficiently strong electron-electron repulsion, quantum spin Hall insulators can undergo a Mott transition to a topologically trivial antiferromagnet without edge states [6]. Quantum Monte Carlo simulations [7–9] of the Kane-Mele-Hubbard model have confirmed the expected 3D XY universality class of this transition, which remains unchanged even for a long-range Coulomb interaction [10]. Correlation effects have been studied in great detail also for other models [11].

Because the bulk of a quantum spin Hall insulator is gapped, the edge states are exponentially localized at the edge. At sufficiently low energies, they may therefore be considered to be one-dimensional. Consequently, the effect of electron-electron interactions cannot be captured using perturbation theory or mean-field methods. Instead, a faithful description of correlated helical edge states is based on the bosonization method [12, 13].

A remarkable theoretical prediction is the occurrence of an edge-Mott transition as a result of strong electron-electron repulsion [14]. Such a transition requires half-filled edge states and a Rashba spin-orbit term to allow umklapp scattering [15]. Whereas the first condition is rather special, the second is generic for experimental realizations. Above a critical interaction (the critical point

corresponds to a Luttinger parameter $K = 1/2$), umklapp scattering is a relevant perturbation, and the edge is expected to exhibit Ising long-range magnetic order and an excitation gap at $T = 0$ [14]. In this scenario, time-reversal symmetry is broken only at the edge while the bulk remains topological, leading to a breakdown of the bulk-boundary correspondence [16–18].

In contrast to the bulk Mott transition, the edge-Mott transition has not been demonstrated numerically. In particular, the Rashba term gives rise to a sign problem that makes quantum Monte Carlo simulations challenging. Previous work on models without Rashba coupling (and hence no Mott transition) revealed a strong suppression (enhancement) of the charge (spin) fluctuations and of the spectral weight at the Fermi level suggestive of a Mott transition [7, 9, 15, 19]. It was also shown that correlation effects are generically stronger at the edges than in the bulk [7, 20], and that the condition $K < 1/2$ for an edge Mott state seems to be fulfilled in large regions of the phase diagram [7, 9, 15]. Correlated edge states were also simulated numerically with quantum cluster methods [21–24], but the latter do not capture the characteristic Luttinger liquid physics. For future experiments, it is interesting to consider how different the signatures of the Mott transition are from generic interaction effects.

Here, we simulate a Kane-Mele-Hubbard model using a quantum Carlo (QMC) method. Because interactions are only taken into account at the edge, the sign problem caused by the Rashba term is not prohibitive. By comparing spin correlation functions and single-particle spectral functions we conclude that for accessible system sizes the differences due to Rashba coupling are much more subtle than expected. The main reason for the absence of striking signatures of this transition is that correlation effects strongly modify the helical edge states even in the absence of a Mott transition.

The rest of this paper is organized as follows. In Sec. II, we discuss the model and the method used. Our results are presented in Sec. III. A discussion of our findings is given in Sec. IV, followed by our conclusions in Sec. V.

II. MODEL

The Kane-Mele-Hubbard model [6] provides a framework to study correlation effects in two-dimensional topological insulators (see Ref. [11] for a review). The Hamiltonian of the underlying Kane-Mele model is [1]

$$H_{\text{KM}} = -t \sum_{\langle i,j \rangle} \hat{c}_i^\dagger \hat{c}_j + i\lambda \sum_{\langle\langle i,j \rangle\rangle} \hat{c}_i^\dagger (\boldsymbol{\nu}_{ij} \cdot \boldsymbol{\sigma}) \hat{c}_j \quad (1)$$

$$+ i\alpha \sum_{\langle i,j \rangle} \hat{c}_i^\dagger (\boldsymbol{\sigma} \times \hat{\mathbf{d}}_{ij}) \cdot \hat{\mathbf{z}} \hat{c}_j,$$

where we have used the spinor notation $\hat{c}_i = (c_{i\uparrow}, c_{i\downarrow})^T$ and the Pauli vector $\boldsymbol{\sigma}$. Hamiltonian (1) consists of the usual tight-binding hopping term familiar from graphene ($\sim t$) [25], the s^z -conserving spin-orbit term first derived by Kane and Mele ($\sim \lambda$) [1], and a Rashba term ($\sim \alpha$) [26]. All three terms correspond to single-electron hopping processes on the honeycomb lattice. The sign of the spin-orbit and Rashba terms depends on the sublattice, the direction of the hop (left or right turn), and the spin. Explicitly, $\boldsymbol{\nu}_{ij} = \mathbf{d}_{ik} \times \mathbf{d}_{kj} / |\mathbf{d}_{ik} \times \mathbf{d}_{kj}|$ and $\hat{\mathbf{d}}_{ij} = \mathbf{d}_{ij} / |\mathbf{d}_{ij}|$, with \mathbf{d}_{ij} being a vector connecting sites i and j , and k the intermediate site on the hopping path from i to j . For $\alpha = 0$, the Kane-Mele model (1) is equivalent to two time-reversed copies of the Haldane model [27].

For $\lambda = \alpha = 0$, Hamiltonian (1) describes a semimetal with a linear spectrum at the Dirac points and a vanishing density of states at the Fermi level [25]. If $\alpha = 0$, the Kane-Mele model has a quantum spin Hall ground state for any $\lambda > 0$, characterized by a Z_2 topological invariant $\nu = 1$, a quantized spin Hall conductivity $\sigma_{xy}^s = \nu e^2 / 2\pi$, and a pair of helical edge states. The Rashba term does not conserve spin [reducing the spin symmetry from $U(1)$ to Z_2], and competes with the λ term. The quantum spin Hall state remains stable up to $\alpha = 2\sqrt{3}\lambda$ [5, 28].

The phase diagram of the Kane-Mele-Hubbard model with an interaction $H_U = \frac{U}{2} \sum_i (\hat{c}_i^\dagger \hat{c}_i - 1)^2$, but without a Rashba term, is known from mean-field theory [6] and QMC simulations [9, 10]. For $\lambda > 0$, the ground state is a quantum spin Hall insulator for $U < U_c(\lambda)$, and an antiferromagnetic insulator with long-range order in the transverse spin direction for $U \geq U_c(\lambda)$. Importantly, the quantum spin Hall state at $U > 0$ is adiabatically connected to the $U = 0$ state [7, 8], and bulk interactions are of minor importance in this gapped phase. While an additional Rashba term competes with the topological band gap induced by the spin-orbit term, recent cluster calculations suggest that the critical U for the bulk Mott transition is only weakly affected [24].

To compare with theoretical predictions, it is necessary to consider sufficiently large ribbons at low temperatures. The ribbon width L_\perp (the extent perpendicular to the edge) has to be large enough to avoid a hybridization of opposite edges [20, 29, 30]. The length L determines the momentum resolution and the maximal length scale for correlations. To compare to the bosonization results,

we want to avoid any approximations that break symmetries or neglect fluctuations. QMC simulations of the full Kane-Mele-Hubbard model cannot take into account a Rashba term due to a sign problem [8]. Therefore, we make use of the previously introduced idea [7, 15] of considering electronic interactions only at the edge, an approximation that is well justified by the absence of low-energy bulk excitations and the exponential localization of the edge states. This simplification allows us to simulate correlated edge states with Rashba coupling on reasonably large lattices. The Rashba term gives rise to a sign problem. However, the latter is not prohibitive here because it depends on the volume of the interacting one-dimensional edge (L) rather than the volume of the two-dimensional ribbon ($L \times L_\perp$). We will show in Sec. III that our simulations reproduce the theoretical predictions, and hence capture the physics of correlated helical liquids. Keeping interactions only at the edge excludes the bulk magnetic transition. The latter is also not described by the strictly one-dimensional bosonization, although it can be incorporated by an *ad hoc* mass term proportional to the bulk magnetization [22].

The Kane-Mele-Hubbard edge model with Rashba coupling is defined by the action

$$S = - \sum_{ij} \int \int_0^\beta d\tau d\tau' \hat{c}_i^\dagger(\tau) \mathbf{G}_0^{-1}(i-j, \tau - \tau') \hat{c}_j(\tau')$$

$$+ \frac{U}{2} \sum_i \int_0^\beta d\tau \left[\hat{c}_i^\dagger(\tau) \hat{c}_i(\tau) - 1 \right]^2, \quad (2)$$

where i, j index edge sites [7, 15], and \mathbf{G}_0 is the 2×2 Nambu Green function matrix of the Kane-Mele model (1) on an $L \times L_\perp$ zigzag ribbon. Equation (2) describes correlated helical edge states of a topological insulator coupled to the two-dimensional, noninteracting bulk. It can be solved exactly using the CT-INT QMC method [31], and the numerical effort is independent of the ribbon width L_\perp [7, 15].

Here, we will use two related variants of the CT-INT method, namely the original, finite-temperature method [31] with inverse temperature β , and a projective formulation [32] with projection parameter θ . Periodic (open) boundary conditions were used in the direction parallel (perpendicular) to the edge.

III. NUMERICAL RESULTS

This section is organized as follows. We first briefly consider the noninteracting case as a reference point for our study of interaction effects. We then study the evolution of the real-space spin and charge correlations as a function of U , before turning to the single-particle spectral function. We use t as the energy unit, set the lattice constant and k_B to one, and consider a half-filled lattice.

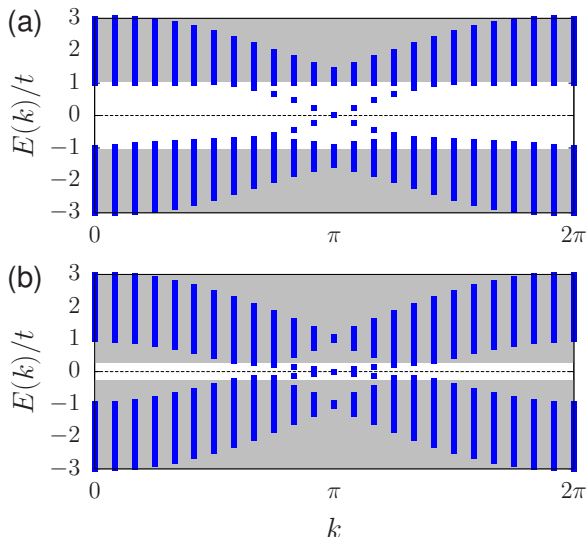


FIG. 1. (Color online) Spectrum of the noninteracting Kane-Mele model on an $L \times L_{\perp}$ zigzag ribbon, showing helical edge states crossing at $k = \pi$. (a) $\lambda/t = 0.2$, (b) $\lambda/t = 0.05$. Here, $\alpha = \lambda$, $L = 24$, and $L_{\perp} = 64$. The shaded areas correspond to bulk states outside the $\alpha = 0$ band gap $\Delta_{\text{SO}} = 3\sqrt{3}\lambda$; the dashed lines indicate the Fermi energy.

A. Noninteracting case

Although we are mostly interested in the regime of strong correlations, the noninteracting case $U = 0$ provides an important limit in which we can verify that (for suitable parameters) our numerical results reproduce the analytical predictions.

Figure 1 shows the eigenvalue spectrum of a zigzag ribbon with dimensions $L \times L_{\perp} = 24 \times 64$, for $\lambda/t = \alpha/t = 0.2$. The ribbon is wide enough to make inter-edge tunneling irrelevant [20, 29, 30]. Figure 1(a) reveals the familiar spin-orbit gap and a pair of helical edge states with a protected crossing at $k = \pi$ [1]. The gap is of the order of t (the exact value for $\alpha = 0$ is $\Delta_{\text{SO}} = 3\sqrt{3}\lambda \approx 1.04t$ [1]). The gray shading indicates the separation between low-energy edge states and high-energy bulk states. The Rashba coupling reduces the band gap [1], and eliminates the particle-hole symmetry. The choice of $\lambda/t = 0.2$ produces a large gap and hence minimizes the impact of the bulk states in simulations, which is crucial to reach the low-energy limit where the bosonization results are valid. In the latter, bulk states are neglected, whereas they are fully taken into account in our simulations. To make the impact of Rashba coupling visible we chose a substantial value $\alpha = \lambda$ that preserves the quantum spin Hall state.

In addition to $\lambda/t = 0.2$, we shall also present selected results for the case $\lambda/t = 0.05$, for which the spectrum is shown in Fig. 1(b). The spin-orbit gap is much smaller ($\Delta_{\text{SO}}/t \approx 0.26$), and the edge states have a significantly smaller velocity. The smaller gap makes it harder to reach the low-energy regime, but the smaller velocity en-

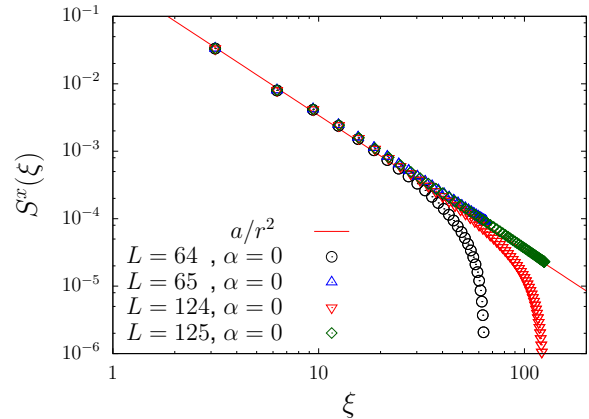


FIG. 2. (Color online) Transverse spin correlations for $U = 0$ and different L . Here, $\lambda/t = 0.2$, $\beta t = 200$, and $L_{\perp} = 64$. The solid line illustrates the expected $1/r^2$ decay.

ables us to simulate stronger correlations. (The relevant parameters controlling correlations are U and the edge state velocity v_F that scales with λ [15].)

For $U = 0$, the amplitude of transverse spin correlations is expected to decay as $1/r^2$ at sufficiently large distances, as follows from the bosonization result

$$S^x(r) = \langle s^x(r)s^x(0) \rangle \sim \cos(2k_F r) r^{-2K} \quad (3)$$

by setting the Luttinger liquid interaction parameter K equal to one. We reproduce this behavior in Fig. 2. To remove the effects of the periodic boundary conditions, we plot the conformal distance [33]

$$\xi = L \sin(\pi r/L). \quad (4)$$

For odd values of the ribbon length L , we indeed find a well-defined power-law decay at large ξ with an exponent very close to 2 both for $L = 65$ and $L = 125$. The expected $1/r^2$ power law is also observed for longitudinal spin correlations (not shown) and charge correlations [Fig. 3(b)]. In contrast, for even values of L , the correlations decay exponentially beyond a certain distance. This odd/even effect has previously been reported in Ref. [19]. Importantly, the helical edge states have a symmetry-protected crossing at $k = \pi$ for even values of L (see Fig. 1). In the following, we use odd L for the calculation of correlation functions, and even L for spectral functions (so that $k = \pi$ is one of the allowed wavevectors).

B. Correlation functions

Having established that we are able to see the power-law correlations theoretically predicted for $U = 0$, we consider the impact of a Hubbard interaction on the real-space spin and charge correlations. The results obtained with the projective CT-INT method are converged within

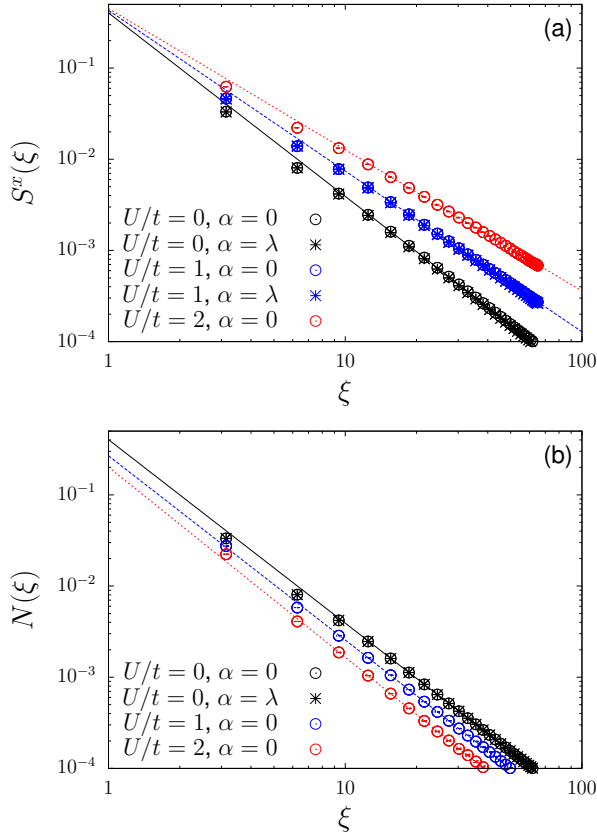


FIG. 3. (Color online) Projective CT-INT results for the transverse spin and charge correlations for different interactions U . Here, $\lambda/t = 0.2$, $L = 65$, $L_{\perp} = 64$, and $\theta t = 40$. Lines are fits to the form a/ξ^{γ} at large distances.

the error bars (if larger than the symbols) or the symbol size, respectively.

We first consider weak and moderately strong interactions on a 65×64 ribbon that is large enough to reveal the asymptotic behavior. Figure 3(a) shows the transverse spin correlator $S^x(\xi)$ for different values of U/t . For $U = 0$, we have the same $1/r^2$ decay as in Fig. 2. With increasing U/t , the transverse spin correlations decay more slowly. Although deviations are visible for small distances, the behavior for $\xi \gtrsim 10$ fits very well to a power-law decay $r^{-\gamma}$ with $\gamma < 2$. The reduction of the exponent as a result of repulsive interactions matches the bosonization result of Eq. (3), where $\gamma = 2K$ and K reduces from $K = 1$ for $U = 0$ to $K < 1$ for $U > 0$. By fitting the decay of $S^x(\xi)$ to the form a/ξ^{γ} at large distances [there are no logarithmic corrections to Eq. (3)], we obtain the estimates $K = 0.882(1)$ for $U/t = 1$ and $K = 0.774(2)$ for $U/t = 2$. The transverse spin correlations are very similar for $\alpha = 0$ and $\alpha = \lambda$. This result is consistent with theoretical predictions: At the Luttinger liquid fixed point, the Rashba coupling scales to zero.

The longitudinal spin correlations and the charge correlations are expected to decay with the same exponent

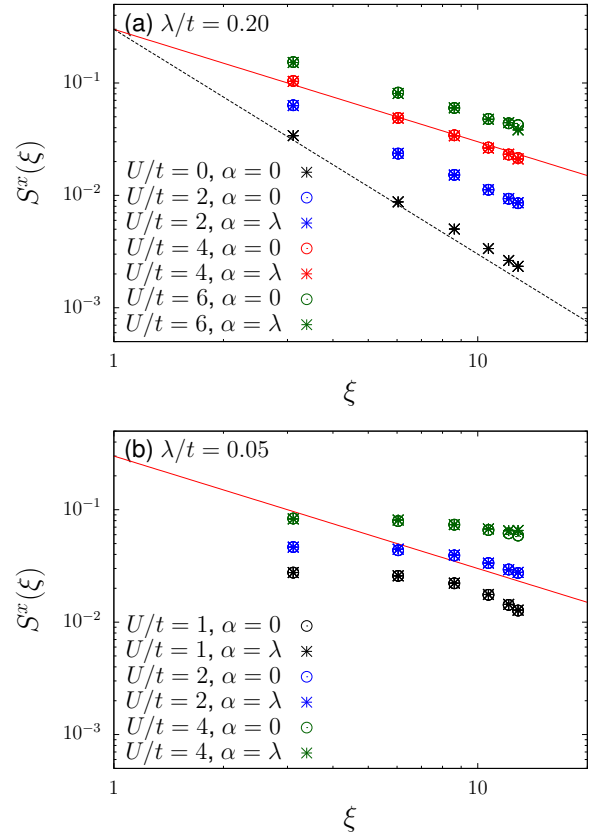


FIG. 4. (Color online) Projective CT-INT results for the transverse spin correlations for different interactions U . Here, $\lambda/t = 0.2$, $L = 13$, $L_{\perp} = 64$, $\theta t = 30$. The dashed (solid) lines illustrate the $1/r^2$ ($1/r$) decay expected for $K = 1$ ($K = 1/2$).

$\gamma = 2$ for any value of U in the Luttinger liquid phase [15]. Hence, we have for the charge correlator

$$N(r) = \langle n(r)n(0) \rangle \sim r^{-2}. \quad (5)$$

Our numerical results for $N(\xi)$ in Fig. 3(b) confirm that the exponent remains unchanged for $U > 0$; the fits to a power-law give $K = 1$ within error bars. The excellent agreement of our results with theoretical predictions illustrates that we can indeed reach the low-energy regime, and that the bosonization results hold even for $U > \Delta_{\text{SO}}$.

Because the numerical effort for simulations with the CT-INT method scales roughly as U^3 [31], we are forced to consider smaller L in the strong-coupling regime (L_{\perp} remains unchanged). Accordingly, Fig. 4 shows the transverse spin correlations for $L = 13$, a system size small enough to reliably calculate the single-particle spectral function below. The exponent for the decay of $S^x(\xi)$ decreases further as we consider larger values of U/t . For $U/t = 4$ and $U/t = 6$ it appears to be smaller than the critical value $\gamma = 1$ (or $K = 1/2$, illustrated by the solid line) expected at the Mott transition. (For $\alpha > 0$, $T = 0$, and half-filling, the smallest possible exponent for power-law correlations is $\gamma = 1$; beyond that, long-range order sets in. In contrast, for $\alpha = 0$, the lower

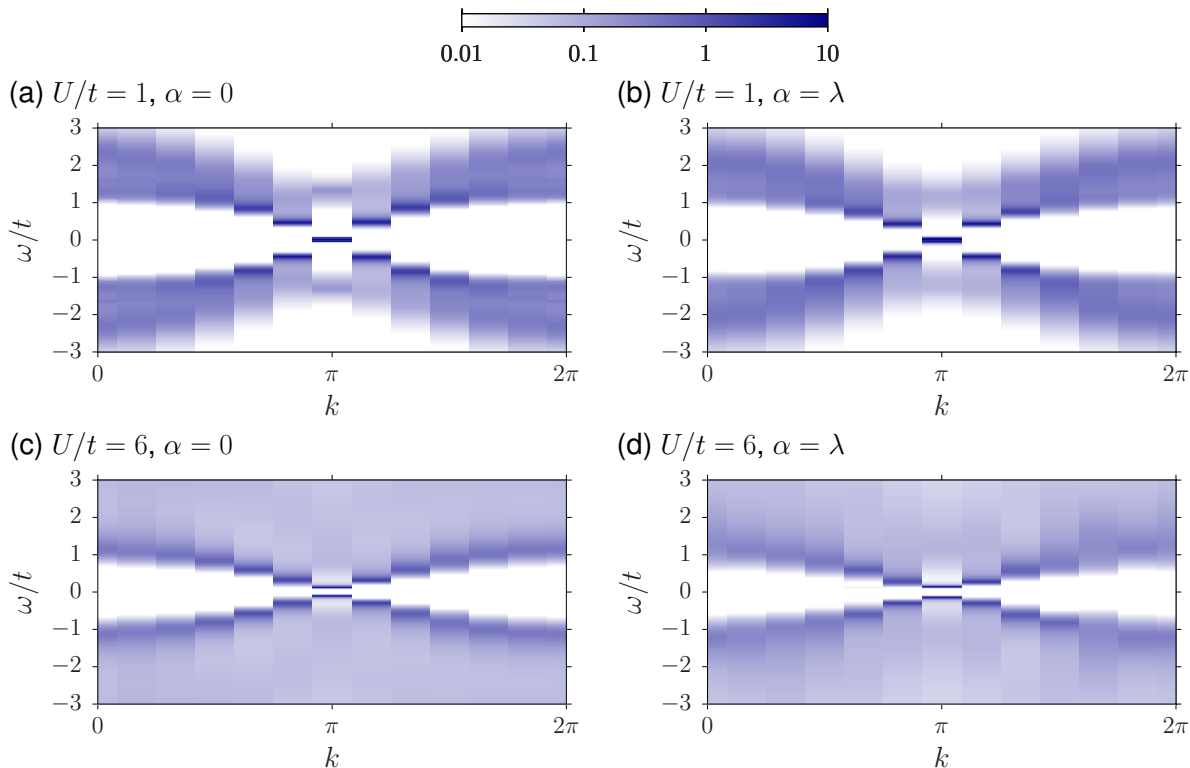


FIG. 5. (Color online) CT-INT results for the single-particle spectral function. Here, $\lambda/t = 0.2$, $L = 12$, $L_{\perp} = 64$, and $\beta t = 60$.

bound is $\gamma = 0$.) The spin correlations are significantly enhanced at a given U for a smaller $\lambda/t = 0.05$, as shown in Fig. 4(b). As pointed out before, correlation effects on the edge states are determined by the ratio U/λ [15].

Figure 3(a) also includes results for a nonzero Rashba coupling $\alpha = \lambda$, which are essentially identical to those for $\alpha = 0$. This suggests that the parameter K is also the same. Clearly, for the system sizes accessible in the strong-coupling regime, we cannot distinguish a slow power-law decay from potential long-range order. However, our results reveal the important fact that there is very little difference between results obtained with and without Rashba coupling.

C. Single-particle spectral function

A key signature of the Mott transition predicted for helical liquids with strong umklapp scattering is the opening of a gap in the single-particle spectrum. As usual for Kosterlitz-Thouless transitions, the gap opens exponentially as a function of U close to the critical point. Moreover, in one dimension, long-range order is only possible at zero temperature.

Here, we calculate the single-particle Green function and the corresponding spectral function at different temperatures. We consider the spin-diagonal and spin-

averaged Green function

$$G(k, \tau) = \frac{1}{2} \left\langle c_{k\uparrow}^{\dagger}(\tau) c_{k\uparrow}(0) + c_{k\downarrow}^{\dagger}(\tau) c_{k\downarrow}(0) \right\rangle \quad (6)$$

from which we obtain the single-particle spectral function

$$A(k, \omega) = -\frac{1}{\pi} \text{Im} G(k, \omega) \quad (7)$$

by inverting the relation (we set $\mu = 0$)

$$G(k, \tau) = \int_{-\infty}^{\infty} d\omega \frac{e^{-\omega\tau}}{1 + e^{-\beta\omega}} A(k, \omega). \quad (8)$$

with the stochastic maximum entropy method [34].

Figure 5 shows results for $\lambda/t = 0.2$ and $\beta t = 60$. We compare the cases of weak and strong interactions, as well as zero and nonzero Rashba coupling. For $U/t = 1$, we see almost identical spectra for $\alpha = 0$ [Fig. 5(a)] and $\alpha = \lambda$ [Fig. 5(b)]. The helical edge states are well visible inside the spin-orbit gap, with a large spectral weight at the Fermi level for $k = \pi$. In the strongly correlated regime, $U/t = 6$, we find a small gap at the Fermi level both for $\alpha = 0$ [Fig. 5(c)] and $\alpha = \lambda$ [Fig. 5(d)].

Figure 6 compares $A(k, \omega)$ for $\lambda/t = 0.2$ and $\lambda/t = 0.05$ in the energy range set by the respective spin-orbit gap Δ_{SO} ; the Rashba coupling has been set to zero. To reveal the interaction effects more clearly, we also include the

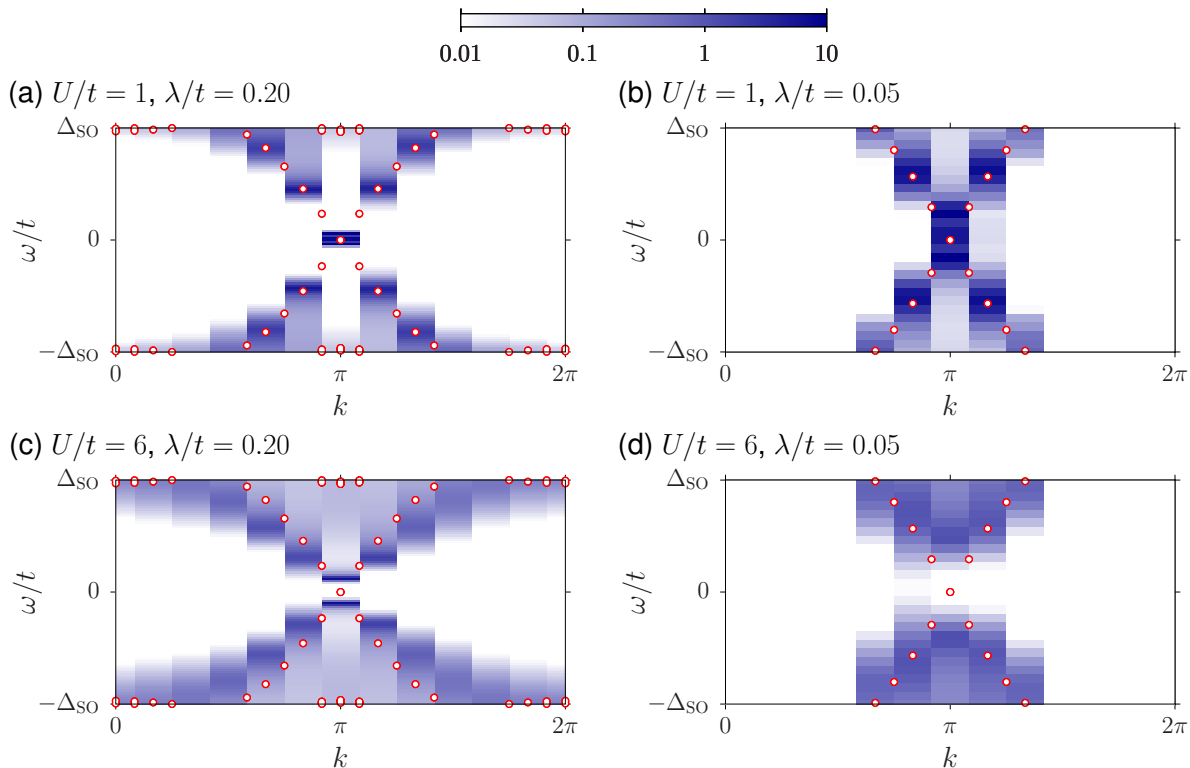


FIG. 6. (Color online) CT-INT results for the single-particle spectral function in the energy range $[-\Delta_{\text{SO}}, \Delta_{\text{SO}}]$, where $\Delta_{\text{SO}} = 3\sqrt{3}\lambda$ is the band gap of the noninteracting model. Here, $\alpha = 0$, $L = 12$, $L_{\perp} = 64$, and $\beta t = 60$. Symbols correspond to the eigenvalues of the noninteracting model with $L = 24$ and $\alpha = 0$ (see also Fig. 1).

noninteracting eigenvalue spectrum (points). Figure 6(a) shows that for $\lambda/t = 0.2$ and $U/t = 1$, the edge states resemble quite closely those of the noninteracting system. In contrast, for $\lambda/t = 0.05$ and $U/t = 1$ (corresponding to roughly a four times larger effective interaction), correlations give rise to a pseudogap at $k = \pi$. This effect is much stronger for $U/t = 6$, as shown in Figs. 6(c) and 6(d). Again, the gap/pseudogap is larger (in units of Δ_{SO}) for the more strongly correlated case of $\lambda/t = 0.05$.

Because the results for the spectral function were obtained on rather small systems ($L = 12$), it is important to investigate finite-size effects. To avoid problems related to the analytic continuation of data with larger statistical errors, we use an alternative way to extract the spectral function at $\omega = 0$ (see also Ref. [35]). Setting $\tau = \beta/2$, we obtain from Eq. (8) the relation

$$\frac{1}{2} \lim_{\beta \rightarrow \infty} \beta G(k, \beta/2) = A(k, 0). \quad (9)$$

In a finite metallic system with a δ peak at $k = k_{\text{F}}$ and $\omega = 0$, $A(k_{\text{F}}, 0)$ and hence $\beta G(k_{\text{F}}, \beta/2)$ diverges in the limit $T \rightarrow 0$. In contrast, in a gapped system, $\beta G(k_{\text{F}}, \beta/2) \rightarrow 0$ as $T \rightarrow 0$.

Figure 7(a) shows $\beta G(k_{\text{F}}, \beta/2)$ (here $k_{\text{F}} = \pi$) as a function of $1/\beta$ for $U/t = 1$. For both $L = 12$ and $L = 20$, $A(k_{\text{F}}, 0)$ increases with decreasing temperature, suggesting the absence of a gap. In contrast, for $U/t = 6$ in

Fig. 7(b), the results for $L = 12$ reveal a gap that is larger for $\alpha = \lambda$ than for $\alpha = 0$, whereas results obtained with and without Rashba coupling are almost identical for $U/t = 1$. These results agree with Fig. 5. Importantly, for $L = 20$, Fig. 7 shows a much larger spectral weight at low temperatures; the data for $\alpha = 0$ even increase with decreasing temperature. This finding suggests that the gap seen in Fig. 5 for strong interactions and $L = 12$ is a finite-size effect. The absence of a gap for weak interactions in Fig. 6(a) (and for the noninteracting case, not shown) implies that the gap visible in, for example, Fig. 6(c) is induced by correlations. A more detailed discussion will be given in Sec. IV.

IV. DISCUSSION

Without Rashba coupling, or away from half-filling, the bosonization results predict that all correlation functions decay with a power law at zero temperature. With increasing U , transverse spin correlations decay more slowly (the exponent is $2K$, with $K < 1$ for $U > 0$), but there is no long-range order. The edge states hence remain gapless, in accordance with the unchanged $1/r^2$ decay of charge correlations. Neglecting the high-energy bulk states, these results hold even for very large U (com-

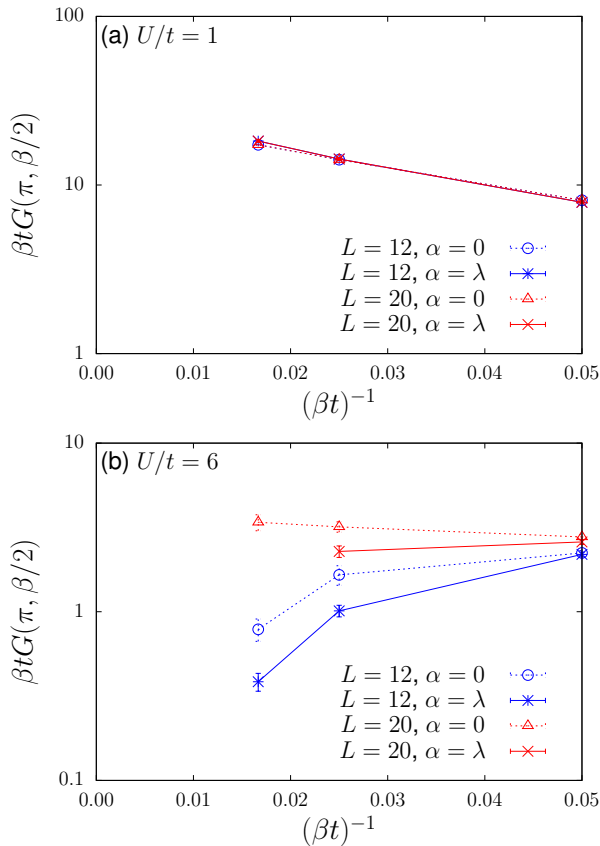


FIG. 7. (Color online) CT-INT results for the rescaled single-particle Green function at $k_F = \pi$, $\tau = \beta/2$. Here, $\lambda/t = 0.2$, $L = 12$, and $L_{\perp} = 64$.

pared to the bulk band gap Δ_{SO}). Importantly, whereas a mean-field treatment of interactions at the edge gives a magnetic state for any $U > 0$, order-parameter fluctuations destroy the long-range order and give rise to power-law correlations even at $T = 0$ [20].

For a helical liquid *with Rashba coupling*, the same physics is expected as long as umklapp scattering is not relevant (i.e., for $K > 1/2$ and/or away from half-filling). For $K < 1/2$ at half-filling, umklapp scattering becomes a relevant perturbation, and drives the system away from the metallic Luttinger liquid fixed point [14]. The system develops long-range magnetic order in the transverse spin direction at $T = 0$, corresponding to a spontaneous symmetry breaking with an Ising (Z_2) order parameter. The helical edge states hence undergo a Mott transition and acquire a gap at the Fermi level. The latter is allowed because the magnetic order breaks the protecting time-reversal symmetry at the edge. In the Mott phase, density fluctuations are exponentially suppressed. At $T > 0$, the long-range order is destroyed by thermally induced fluctuations of the order parameter, and time-reversal symmetry is restored. We can think of the ordered state in terms of a scalar field. The order parameter correlation length (the average distance between thermally induced

domain walls) decreases exponentially with increasing temperature. Similar to solitons in the Su-Schrieffer-Heeger model [36], domain walls (kinks) correspond to midgap states, and the single-particle gap is filled in at $T > 0$.

Let us compare these theoretical predictions with the numerical results presented in Sec. III. Figure 2 demonstrates that, for not too large values of U , our simulations capture the low-energy and long-wavelength limit where the bosonization results of Eqs. (3) and (5) hold. A power-law decay persists even when U becomes larger than the spin-orbit gap, although deviations can be observed when $U \gg \Delta_{\text{SO}}$. For $\lambda/t = 0.2$ and $U/t \leq 2$, corresponding to the Luttinger liquid regime with $K > 1/2$, the results are almost unaffected by Rashba coupling, which is an irrelevant perturbation at the Luttinger liquid fixed point. Transverse spin correlations are strongly enhanced with increasing U , with U/λ being the relevant parameter ratio for the low-energy physics.

For large U/λ , spin correlations decay increasingly slowly both with or without Rashba coupling. Although theory predicts a gapless Luttinger liquid even at $T = 0$, we observe a gap in the single-particle spectrum at low but finite temperatures. This gap decreases with increasing system size, and is expected to close in the thermodynamic limit. However, the accessible system sizes are insufficient to capture the quantum fluctuations of the order parameter that destroy the long-range order induced by the mean-field instability [20]. By this mechanism, we observe a single-particle gap even without a Rashba term that becomes larger (for a given system size) with increasing U/λ . Similarly, a gap is observed with Rashba coupling at $T > 0$ for small system sizes. While spin correlations are very similar with and without Rashba coupling, the spectral weight at the Fermi level is more strongly suppressed in the presence of Rashba coupling.

The generic strong spin correlations and mean-field instability of helical liquids—both of which are not specific to half-filling—make it very difficult to observe clear signatures of the umklapp-induced Mott transition numerically. In addition to the quasi-long-range order of spins, it has been previously shown that the spectral weight at the Fermi level is suppressed by spin-flip scattering involving bulk states [15, 19], giving rise to a pseudogap. Distinguishing quasi-long-range order [$K \ll 1$ in Eq. (3)] and a pseudogap for $\alpha = 0$ from long-range order and a gap for $\alpha > 0$ is very difficult.

The Mott transition in helical liquids is expected to become visible in simulations on much larger two-dimensional lattices and at zero temperature, for which suitable methods will have to be developed. A possible route toward this goal is tensor networks, which have recently been applied to quantum Hall systems [11, 37]. Other promising ways to detect the Mott transition numerically include the calculation of the edge topological invariant [18] or the entanglement entropy [38], both of which are qualitatively (rather than quantitatively) different in the ordered and disordered phases, respectively.

V. CONCLUSIONS

We studied the role of Rashba coupling for helical edge states of quantum spin Hall insulators by simulating a Kane-Mele model with a Hubbard interaction at the edge using quantum Monte Carlo methods. We were able to reveal the theoretically predicted asymptotic behavior of spin and charge correlation functions. Because of limitations in system size, we observed an interaction-induced single-particle gap at strong interactions, which is expected to close or be filled in in the thermodynamic limit at any finite temperature. Quite surprisingly, our numerical data are very similar for models with and without Rashba coupling, although the latter allows for a Mott state with long-range magnetic order at zero temperature that breaks time-reversal symmetry.

Our observation of a gap for large U can be attributed to the fact that in the regime where a Mott state can exist ($K < 1/2$), spin correlations decay slower than $1/r$. On finite lattices, such a slow decay is difficult to distinguish from mean-field order. Put differently, the order parameter fluctuations that destroy the magnetic order

for $K > 1/2$ and $T = 0$ or for $K < 1/2$ and $T > 0$ involve length scales that are not fully captured by the accessible system sizes. Hence, whereas numerical work has successfully linked Mott transitions in other one- and two-dimensional models to theoretical predictions, the Mott transition of a helical Luttinger liquid appears to be out of reach for existing numerical methods.

While the requirement of half-filling at first suggests that the Mott transition is not particularly relevant for experiments, our results reveal that correlated helical edge states exhibit many of the characteristics of finite-temperature Mott states (pronounced spin correlations, suppressed spectral weight at the Fermi level) even when a Mott transition is not allowed.

ACKNOWLEDGMENTS

We are grateful to the Jülich Supercomputing Centre for computer time, and acknowledge financial support from the DFG Grants Nos. AS120/9-1 and Ho 4489/3-1 (FOR 1807). We further thank L. Fritz and S. Rachel for helpful discussions during the SPORE13 workshop.

-
- ¹ C. L. Kane and E. J. Mele, Phys. Rev. Lett. **95**, 146802 (2005); *ibid* **95**, 226801 (2005).
- ² M. Z. Hasan and C. L. Kane, Rev. Mod. Phys. **82**, 3045 (2010).
- ³ B. A. Bernevig, T. L. Hughes, and S. Zhang, Science **314**, 1757 (2006).
- ⁴ M. König, S. Wiedmann, C. Brüne, A. Roth, H. Buhmann, L. W. Molenkamp, X.-L. Qi, and S.-C. Zhang, Science **318**, 766 (2007).
- ⁵ L. Sheng, D. N. Sheng, C. S. Ting, and F. D. M. Haldane, Phys. Rev. Lett. **95**, 136602 (2005).
- ⁶ S. Rachel and K. Le Hur, Phys. Rev. B **82**, 075106 (2010).
- ⁷ M. Hohenadler, T. C. Lang, and F. F. Assaad, Phys. Rev. Lett. **106**, 100403 (2011); **109**, 229902(E) (2012).
- ⁸ M. Hohenadler, Z. Y. Meng, T. C. Lang, S. Wessel, A. Muramatsu, and F. F. Assaad, Phys. Rev. B **85**, 115132 (2012).
- ⁹ D. Zheng, G.-M. Zhang, and C. Wu, Phys. Rev. B **84**, 205121 (2011).
- ¹⁰ M. Hohenadler, F. Parisen Toldin, I. F. Herbut, and F. F. Assaad, Phys. Rev. B **90**, 085146 (2014).
- ¹¹ M. Hohenadler and F. F. Assaad, J. Phys.: Condens. Matter **25**, 143201 (2013).
- ¹² J. Voit, Rep. Prog. Phys. **57**, 977 (1994).
- ¹³ T. Giamarchi, *Quantum Physics in One Dimension* (Clarendon Press, Oxford, 2004), ISBN 0 19 85 25 00 1.
- ¹⁴ C. Wu, B. A. Bernevig, and S.-C. Zhang, Phys. Rev. Lett. **96**, 106401 (2006).
- ¹⁵ M. Hohenadler and F. F. Assaad, Phys. Rev. B **85**, 081106 (2012); **86**, 199901(E) (2012).
- ¹⁶ L. Fu and C. L. Kane, Phys. Rev. B **74**, 195312 (2006).
- ¹⁷ X.-L. Qi, Y.-S. Wu, and S.-C. Zhang, Phys. Rev. B **74**, 045125 (2006).
- ¹⁸ V. Gurarie, Phys. Rev. B **83**, 085426 (2011).
- ¹⁹ Y. Yamaji and M. Imada, Phys. Rev. B **83**, 205122 (2011).
- ²⁰ D.-H. Lee, Phys. Rev. Lett. **107**, 166806 (2011).
- ²¹ S.-L. Yu, X. C. Xie, and J.-X. Li, Phys. Rev. Lett. **107**, 010401 (2011).
- ²² W. Wu, S. Rachel, W.-M. Liu, and K. Le Hur, Phys. Rev. B **85**, 205102 (2012).
- ²³ L. Wang, X. Dai, and X. C. Xie, Eur. Phys. Lett. **98**, 57001 (2012).
- ²⁴ M. Laubach, J. Reuther, R. Thomale, and S. Rachel, Phys. Rev. B **90**, 165136 (2014).
- ²⁵ A. H. Castro Neto, F. Guinea, N. M. R. Peres, K. S. Novoselov, and A. K. Geim, Rev. Mod. Phys. **81**, 109 (2009).
- ²⁶ Y. A. Bychkov and E. I. Rashba, J. Phys. C: Solid State Phys. **17**, 6039 (1984).
- ²⁷ F. D. M. Haldane, Phys. Rev. Lett. **61**, 2015 (1988).
- ²⁸ D. N. Sheng, Z. Y. Weng, L. Sheng, and F. D. M. Haldane, Phys. Rev. Lett. **97**, 036808 (2006).
- ²⁹ Y. Tanaka and N. Nagaosa, Phys. Rev. Lett. **103**, 166403 (2009).
- ³⁰ Y. Tada, R. Peters, M. Oshikawa, A. Koga, N. Kawakami, and S. Fujimoto, Phys. Rev. B **85**, 165138 (2012).
- ³¹ A. N. Rubtsov, V. V. Savkin, and A. I. Lichtenstein, Phys. Rev. B **72**, 035122 (2005).
- ³² F. F. Assaad and T. C. Lang, Phys. Rev. B **76**, 035116 (2007).
- ³³ J. Cardy, *Scaling and Renormalization in Statistical Physics* (Cambridge University Press, Cambridge, 1996).
- ³⁴ K. S. D. Beach, arXiv:0403055.
- ³⁵ R. T. Scalettar, N. Trivedi, and C. Huscroft, Phys. Rev. B **59**, 4364 (1999).
- ³⁶ W. P. Su, J. R. Schrieffer, and A. J. Heeger, Phys. Rev. B **22**, 2099 (1980).
- ³⁷ B. Béri and N. R. Cooper, Phys. Rev. Lett. **106**, 156401 (2011).
- ³⁸ G. Vidal, J. I. Latorre, E. Rico, and A. Kitaev, Phys. Rev. Lett. **90**, 227902 (2003).